Materials Today Physics 32 (2023) 101031

Contents lists available at ScienceDirect

Materials Today Physics

journal homepage: www.journals.elsevier.com/materials-today-physics

The emergence of considerable room temperature magnetocaloric performances in the transition metal high-entropy alloys

Yikun Zhang [a,b], Peng Xu [a], Jian Zhu [b], Shiming Yan [a], Jincang Zhang [c], Lingwei Li [a,*]

[a] School of Electronics and Information & Key Laboratory of Novel Materials for Sensor of Zhejiang Province, Hangzhou Dianzi University, Hangzhou, 310012, China
[b] State Key Laboratory of Advanced Special Steels, Shanghai University, Shanghai, 200444, China
[c] Zhejiang Laboratory, Hangzhou, 311100, China

ARTICLE INFO

Keywords:
Magnetocaloric performances
Transition metal high entropy alloys
Magnetic properties
Mechanical properties
Room temperature magnetic refrigeration

ABSTRACT

We herein investigated the structural, magnetic, and magnetocaloric properties of $Mn_{20}Al_{20}Co_{14}Fe_{20+x}Cr_{26-x}$high entropy (HE) alloys by experimental determination and first principle calculations. The results indicated that these alloys were crystallized in a disordered body-centered cubic structure.The Fe substitution of Cr enhanced the energy and net magnetic moment of these alloys, resulting in the improvement of magnetic properties. All the $Mn_{20}Al_{20}Co_{14}Fe_{20+x}Cr_{26-x}$ HE alloys underwent a second-order magnetic transition with theCurie temperature ranges of 268.2–310.6 K. The magnetocaloric performances of $Mn_{20}Al_{20}Co_{14}Fe_{20+x}Cr_{26-x}$ HE alloys were examined by using the magnetic entropy change, relative cooling power, refrigerant capacity, temperature average entropy change, and mechanical properties, which are superior to the reported transition metal-based magnetocaloric materials with second order magnetic phase transition. By considering the realized considerablemagnetocaloricperformances and the benefits of transition metal HE alloys, the present $Mn_{20}Al_{20}Co_{14}Fe_{20+x}Cr_{26-x}$ HE alloys are also of potential for room temperature MR application. The present work would provide a large family of transition metal HE alloys with significant magnetocaloric performances.

1. Introduction

Discovering new classes of novel functional materials with significant tailorable performance has significant potential for further technological improvements and breakthroughs. Among these, magnetic materials exhibiting highly specific properties, including spin polarization, certain magnetic phase transitions, and high magnetization, have attracted much research interest [1–10]. Responsibly addressing the effects of contemporary life on climate change is urgent. Solid-state magnetic refrigeration (MR) is an emerging environmentally friendly technology with the potential to replace the commonly used vapor-cycle cooling since it has rewritten long-established technology standards [1–5]. MR is based on magnetocaloric effect (MCE), an inherent magnetic field inducing the reversible temperature changes of the materials by the variation in magnetic field. Therefore, a crucial prerequisite for MR application is exploring magnetic substances with excellent magnetocaloric performances. Such magnetic substances must satisfy a wide range of criteria, including large values of isothermal magnetic entropy changes (ΔS_M) and adiabatic temperature changes (ΔT_{ad}), high relative cooling powers (*RCP*) and refrigerant capacity (*RC*), a proper magnetic phase transition (MPT) temperature and wide working temperature range, good reversibility and sensitivity to an applied low magnetic field [1–5]. In the past few decades, much effort has been made to explore MC materials. Thus, many potentially suitable materials were identified, such as pure Gd-based materials, Ni–Mn-based Heusler type alloys, La–Fe–Si-based alloys, and some rare earth (*RE*)-based alloys or compounds [1–5,11–22]. Currently, the most commonly used magnetocaloric materials for room temperature MR applications are pure Gd-based and La–Fe–Si-based materials. However, the high cost of the former and the poor mechanical properties of the latter have been major obstacles to upscaling to mass production.

Recently, a distinct and emergent material design strategy has been introduced to develop novel materials, i.e. the high-entropy (HE) alloys [23–27], which consists of multiple principle elements yielding high configurational entropy, unlike the conventional material containing only one principle element. The HE alloys have received increasing research interests because they have opened a near-infinite compositional space for designing materials with a remarkable combination of structural, chemical, and physical properties. In the past few decades, successive efforts have mainly focused on elaborating their

* Corresponding author. .
E-mail address: lingwei@hdu.edu.cn (L. Li).

https://doi.org/10.1016/j.mtphys.2023.101031
Received 27 November 2022; Received in revised form 21 February 2023; Accepted 28 February 2023
Available online 1 March 2023

microstructural and mechanical properties to explore the potential application of HE alloys as structural materials. There are three main types of classic simple crystal structures in HE alloys: face-centered cubic (fcc), body-centered cubic (bcc), and hexagonal close packing (hcp). Superior mechanical properties have been achieved in some HE alloys [25–27] by tuning their chemical compositions and phase structures. Moreover, some research exploring the functional properties of HE alloys, and also including the MCE [28–39], have been recently focused. A detailed comparison of the magnetocaloric performances of the reported HE alloys can be found in the very recently published review papers by Law et al. [30,32]. Notably, the transition metal HE alloys have been considered the most promising because a wide variety of HE alloys have mainly relied on transition metals, which can provide flexible, tunable magnetic and magnetocaloric properties, as well as good corrosion at a low cost.

Inspired by impressive progress in using HE alloys for MR, we have developed novel magnetocaloric materials. In this work, we identified a family of $Mn_{20}Al_{20}Co_{14}Fe_{20+x}Cr_{26-x}$ transition metal high-entropy (HE) alloys with significant room temperature magnetocaloric performances by varying the Fe/Cr ratio. A combination of experimental and computational investigations was performed to elucidate their magnetic and MC properties. The results demonstrated that single bcc-phased $Mn_{20}Al_{20}Co_{14}Fe_{20+x}Cr_{26-x}$HE alloys could bring subnational magnetocaloric performances with a wide MPT temperature span covering room temperature. This finding could provide meaningful insight into the design and exploration of magnetic HE alloys for practical room temperature MR applications.

2. Experimental and calculation details

Samples with compositions of $Mn_{20}Al_{20}Co_{14}Fe_{20+x}Cr_{26-x}$($x = 0$, 1, 2, 3) were prepared by arc-melting the consistent elements with purities greater than 99.9 wt% under an Ar-controlled atmosphere in the presence of a Ti getter. Each sample was flipped and then re-melted another three times to achieve better homogeneity. Then, the samples were noted as $Fe_{20}Cr_{26}$, $Fe_{21}Cr_{25}$, $Fe_{22}Cr_{24}$, and $Fe_{23}Cr_{23}$ for $x = 0$, 1, 2, and 3, according to their Fe and Cr contents, respectively. The phase compositions of the $Mn_{20}Al_{20}Co_{14}Fe_{20+x}Cr_{26-x}$ HE alloys were characterized by a Rigaku SmartLab X-ray diffraction (XRD, Cu-*K*α).The microstructure and bulk chemical compositions of these alloys were characterized from their cross-sections using the scanning electron microscope (SEM) equipped with energy-dispersion X-ray spectroscopy (EDS) mapping on an SM-7800F using an accelerating voltage of 20 kV. The magnetization measurements of present HE alloys were conducted by the magnetic property measurement system (MPMSQ3) from Quantum Design.

The *ab initio* calculations of the ground state electronic and magnetic properties for the $Mn_{20}Al_{20}Co_{14}Fe_{20+x}Cr_{26-x}$ HE alloys were determined with first principle calculation with the assistance of a Vienna *ab initio* Simulation Package (VASP) [40]. A plane-wave code with a projector-augmented wave (PAW) approach and a Perdew-Burke-Ernzerhof (PBE) exchange–correlation functional of spin-polarized generalized gradient approximation (GGA) [41,42] were used to describe the interaction between ions and electrons. Moreover, we performed an approximate calculation of$Mn_{20}Al_{20}Co_{14}Fe_{20+x}Cr_{26-x}$ HE alloys by constructing a supercell and scrambling the atomic positions with random arrangement, which is similar to previous investigations by Wei et al. [43] and Jung et al. [44]. Firstly, the supercell contains 100 atomic coordinates with bcc order was constructed. Then, 100 fixed elementatoms of Mn, Al, Co, Fe and Cr with the fixed ratio of 20: 20: 14: 20 + x: 26-x are allocatedin a randomly disorder arrangement, which corresponds to the ordered coordinates. Therefore, the structural information of atoms random arrangement has been obtained. On the basis of these structural characteristics, the magnetic parameters including the atomic magnetic moment and the charge density were calculated by aid of the VASP software. A plane wave basis cutoff energy of 520 eV was set for all calculations to minimize the force of each atom and stress tensor. The Monkhorst-Pack method was employed to sample the Brillouin zone. The *k*-points 2 × 1 × 1 and 3 × 1 × 1 were applied to calculate the total energies and the density of states (DOS), respectively. The energy convergence criteria within 1 meV and 0.01 eV/Å for the total energies and the total atomic forces were established.

3. Results and discussion

Fig. 1(a) presents the room temperature XRD patterns and the corresponding Miller indices of the $Mn_{20}Al_{20}Co_{14}Fe_{20+x}Cr_{26-x}$ HE alloys. The identifying phase was then conducted. Except of small amount impurity σ phase for $Fe_{23}Cr_{23}$, as indicated in Fig. 1(a), the studied samples show the bcc structure at room temperature. The values of lattice parameter a, as presented in Table 1, is slightly decreased with increasing Cr content from 2.8918 for $Fe_{20}Cr_{26}$ to 2.8902 for $Fe_{22}Cr_{24}$, which is due to the fact of smaller ionic radius of Cr than Fe. The representative SEM backscattered electron image (BSE) images and EDS mapping results of all the $Mn_{20}Al_{20}Co_{14}Fe_{20+x}Cr_{26-x}$HE alloys were characterized, all the alloys show quite similar behaviors and the images for $Fe_{22}Cr_{24}$ are presented in Fig. 1(b) as examples. The microstructure on the entire surface of each sample was homogeneous, and no observable secondary phases could be noted, which is comparable to the XRD results. Moreover, the EDS elements mapping of Mn, Al, Co, Fe, and Cr were also determined, which could provide a visual, direct observation of micro-scale compositional homogeneity. The EDS mapping results, as presented in Fig. 1(b), verified that all the elements in the four studied samples were homogeneously distributed at the micrometer scale. The resulted mean elemental ratios of the Mn, Al, Co, Fe, and Cr elements are summarized in Table 1. The overall compositions of the present $Mn_{20}Al_{20}Co_{14}Fe_{20+x}Cr_{26-x}$ HE alloys were close to their respective nominal compositions.

Fig. 1(c) presents the temperature (T) dependent magnetization (M) of the $Mn_{20}Al_{20}Co_{14}Fe_{20+x}Cr_{26-x}$ HE alloys under the applied magnetic field (H) of 0.01 T. A typical ferromagnetic (FM) to paramagnetic (PM) phase transition can be observed in the HE alloys. The evaluated values of Curie temperatures (T_C, as listed in Table 1), based on the minimum of the derivation from the dM/dT versus T curve rapidly increasing with increasing Fe/Cr ratio, as highlighted in the inset of Fig. 1(c). The $M(T)$ results showed that the Fe contentsignificantly influenced the T_C. The effect of composition variations on magnetic transition temperatures has been observed in some alloys [44–46]. To clearly understand this point, we calculated the total energy difference (ΔE) between the standard magnetic state and the paramagnetic magnetic state for the $Mn_{20}Al_{20}Co_{14}Fe_{20+x}Cr_{26-x}$ HE alloys using VASP software and setting the ISPIN equal to 1. The relationship between ΔE and T_C can be expressed based on the Heisenberg model and Stoner theory [46–48]:

$$\Delta E = -\kappa_b T_C \xi, \quad (1)$$

where ξ is the ratio of M/M_0, M is the magnetic moment at $T \neq 0$ K, and M_0 is the equilibrium magnetic moment at $T = 0$ K, with ξ considered an approximate constant. The T_C (left-scale) and ΔE (right-scale) as a function of Fe content are shown in Fig. 1(d). Notably, there was a common feature of T_C and ΔE with Fe content: i.e. T_C and ΔE both indicated an increasing trend with increasing Fe content. Thus, the Fe substitution of Cr enhanced the energy of the $Mn_{20}Al_{20}Co_{14}Fe_{20+x}Cr_{26-x}$ HE alloys, which resulted in an apparent increase of T_C with increasing Fe content.

To understand and reveal the intrinsic physics behind the alloying elements and their effect on the magnetic state, the density of states (DOS) of the $Mn_{20}Al_{20}Co_{14}Fe_{20+x}Cr_{26-x}$ HE alloys were calculated, as shown in Fig. 2. The Fe and Co atoms made a substantially stronger contribution to the magnetic moment and exhibited higher spin-up than spin-down distributions for each alloy, as represented in Fig. 2(i)–(l) and Fig. 2 (m)–(p). Similarly, Mn atoms showed a higher spin-up distribution (as shown in Fig. 2 (e)–(h)). Therefore, the magnetic moment of Mn

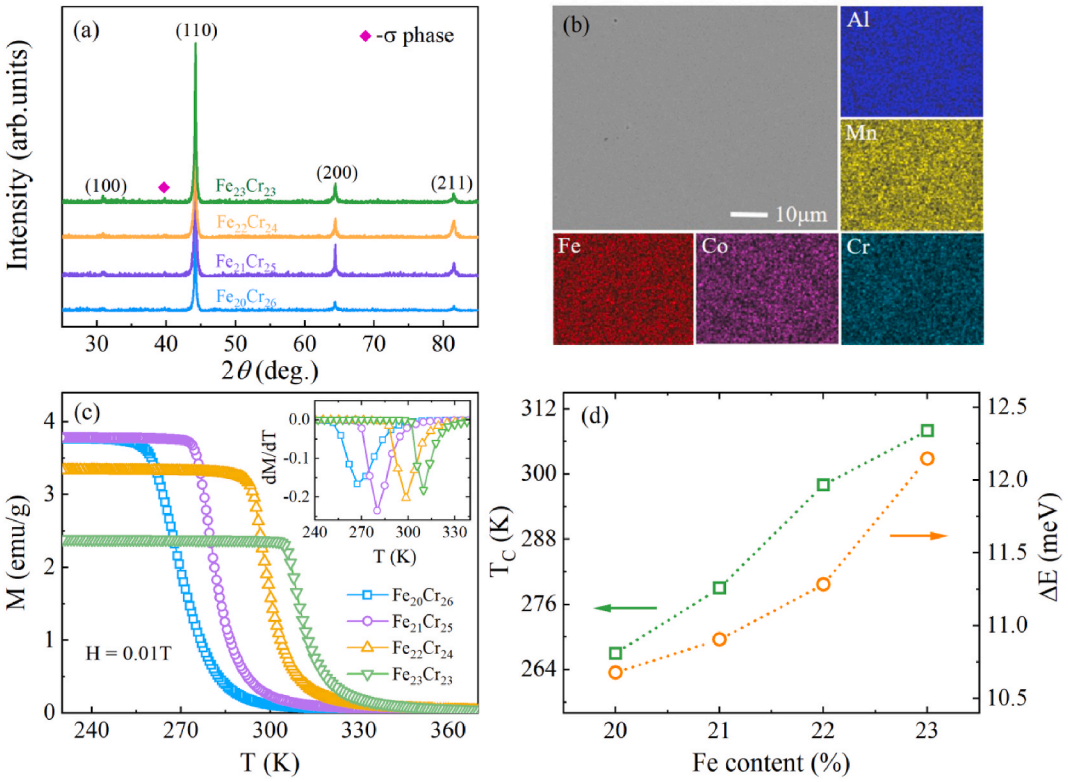

Fig. 1. (a):The room temperature XRDpatternsof$Mn_{20}Al_{20}Co_{14}Fe_{20+x}Cr_{26-x}$ HE alloys. (b): The SEM images and the corresponding distributions of the Mn, Al, Co, Fe, and Cr elements of$Fe_{22}Cr_{24}$HE alloy. (c): The $M(T)$of$Mn_{20}Al_{20}Co_{14}Fe_{20+x}Cr_{26-x}$ HE alloysunder a magnetic field of 0.01 T, the inset shows the corresponding dM/dT versus T curves. (d):The T_C (left-scale) and energy difference ΔE (right-scale) as a function of the Fe contentof $Mn_{20}Al_{20}Co_{14}Fe_{20+x}Cr_{26-x}$ HE alloys.

Table 1
The lattice parameter and mean elemental ratiosof$Mn_{20}Al_{20}Co_{14}Fe_{20+x}Cr_{26-x}$ HE alloys.

Sample	a (Å)	Mn (at. %)	Al (at. %)	Co (at. %)	Fe (at. %)	Cr (at. %)
$Fe_{20}Cr_{26}$	2.8918	19.80	19.74	13.98	20.06	26.42
$Fe_{21}Cr_{25}$	2.8916	19.95	20.03	13.85	21.14	25.03
$Fe_{22}Cr_{24}$	2.8902	20.01	19.89	14.06	22.18	23.86
$Fe_{23}Cr_{23}$	2.8913	19.87	19.98	14.04	22.92	23.19

atoms were parallel to that of Co and Fe atoms, which resulted an increment of the net magnetic moments. To further understand the origin of the high spin moment of Mn atoms, similar with those in AlFeCoCrMn HE alloys [44], the PDOS of Mn in present $Mn_{20}Al_{20}Co_{14}Fe_{20+x}Cr_{26-x}$ HE alloys were also decomposed into e_g (d_{z2}, d_{x2-y2}) t_{2g} and (d_{xy}, d_{yz} and d_{xz}) orbitals for calculation. Consequently, an exchange splitting characteristic for the e_g and t_{2g} orbitals can be found, thus, the obtained large magnetic moment and spin polarization at the Fermi level of Mn are likely due to its d-orbitals splitting. The PDOS of the Cr atoms exhibited higher spin-down than spin-up distributions, which resulted in the decreases of net magnetic moment due to the antiparallel alignments of magnetic moment of the Cr atoms with regard to Co and Fe atoms. Additionally, some slight differences could be noted in the PDOS of the Fe and Cr atoms with increasing Fe content (as shown in Fig. 2 (i)–(l)), which is likely the main reason for the magnetic moment variation of the total system.

Furthermore, in order to provide evidence for the experimental results and to elucidate the change of saturation magnetization, the magnetic moments of the atoms were calculated. The magnetic moment of each atom was extracted, which corresponded to the sequence of ordered coordinates in the constructed supercell. The resulted atomic magnetic moments exhibited somescattered pointsbased on the number and sequence of elements of all the consistent elementsof the $Mn_{20}Al_{20}Co_{14}Fe_{20+x}Cr_{26-x}$ HE alloys, as shown in Fig. 3. The calculated net magnetic moment increases gradually with decreasing Cr content which are 83.55, 85.49, 87.40, and 89.61 Bohr magnetonfor the $Fe_{20}Cr_{26}$, $Fe_{21}Cr_{25}$, $Fe_{22}Cr_{24}$, and $Fe_{23}Cr_{23}$ HE alloys, respectively. Moreover, we can note that the magnetic moment of Al atoms is close to zero. The Mn atoms had highest average magnetic moments, with corresponding values of 2.012, 2.005, 1.993, and 2.003 Bohr magneton for the $Fe_{20}Cr_{26}$, $Fe_{21}Cr_{25}$, $Fe_{22}Cr_{24}$, and $Fe_{23}Cr_{23}$ HE alloys, respectively. These behaviors should be ascribed to the previously described significant d-orbital exchange splitting. Like the Mn atoms, the Fe atoms possessed high average magnetic moments and gradually increased in relation to increasing Fe content, with values of 1.975, 1.978, 1.992, and 2.011 Bohr magneton for the $Fe_{20}Cr_{26}$, $Fe_{21}Cr_{25}$, $Fe_{22}Cr_{24}$, and $Fe_{23}Cr_{23}$ HE alloys, respectively. The corresponding values of the average magnetic moment of Co atoms were 1.281, 1.280, 1.280, and 1.285 Bohr magneton, which were lower than those of the Mn and Fe atoms. Notably, the magnetic moments of the Cr atoms had both positive and negative values. The numbers of magnetic moments for the Cr atoms that antiparallel aligned with Co, Mn, and Fe atoms was obvious more than those of with parallel aligned, therefore a reduction of the net magnetic moment for present $Mn_{20}Al_{20}Co_{14}Fe_{20+x}Cr_{26-x}$ HE alloys.

To elucidate magnetic and magnetic transition behaviors, the field-dependent isothermal magnetization $M(H)$ of the $Mn_{20}Al_{20}Co_{14}Fe_{20+x}Cr_{26-x}$ HE alloys was recorded at fixed temperatures around their T_C. The $M(H)$ curves of all the $Mn_{20}Al_{20}Co_{14}Fe_{20+x}Cr_{26-x}$HE alloys behaved similarly. For clarify, here the selected$M(H)$ curves at 3 K as well as around its own T_C of $Fe_{20}Cr_{26}$and $Fe_{23}Cr_{23}$HE alloys are shown in Fig. 4 (a) and (c), respectively.The magnetic moment at 3 K and 5 T are 43.22, 50.60, 49.31, and 55.99Bohr magneton for the $Fe_{20}Cr_{26}$, $Fe_{21}Cr_{25}$, $Fe_{22}Cr_{24}$, and $Fe_{23}Cr_{23}$ HE alloys, respectively. These experimentally results show same change trend with the theoretically calculated results but the values are obviously smaller than those of the

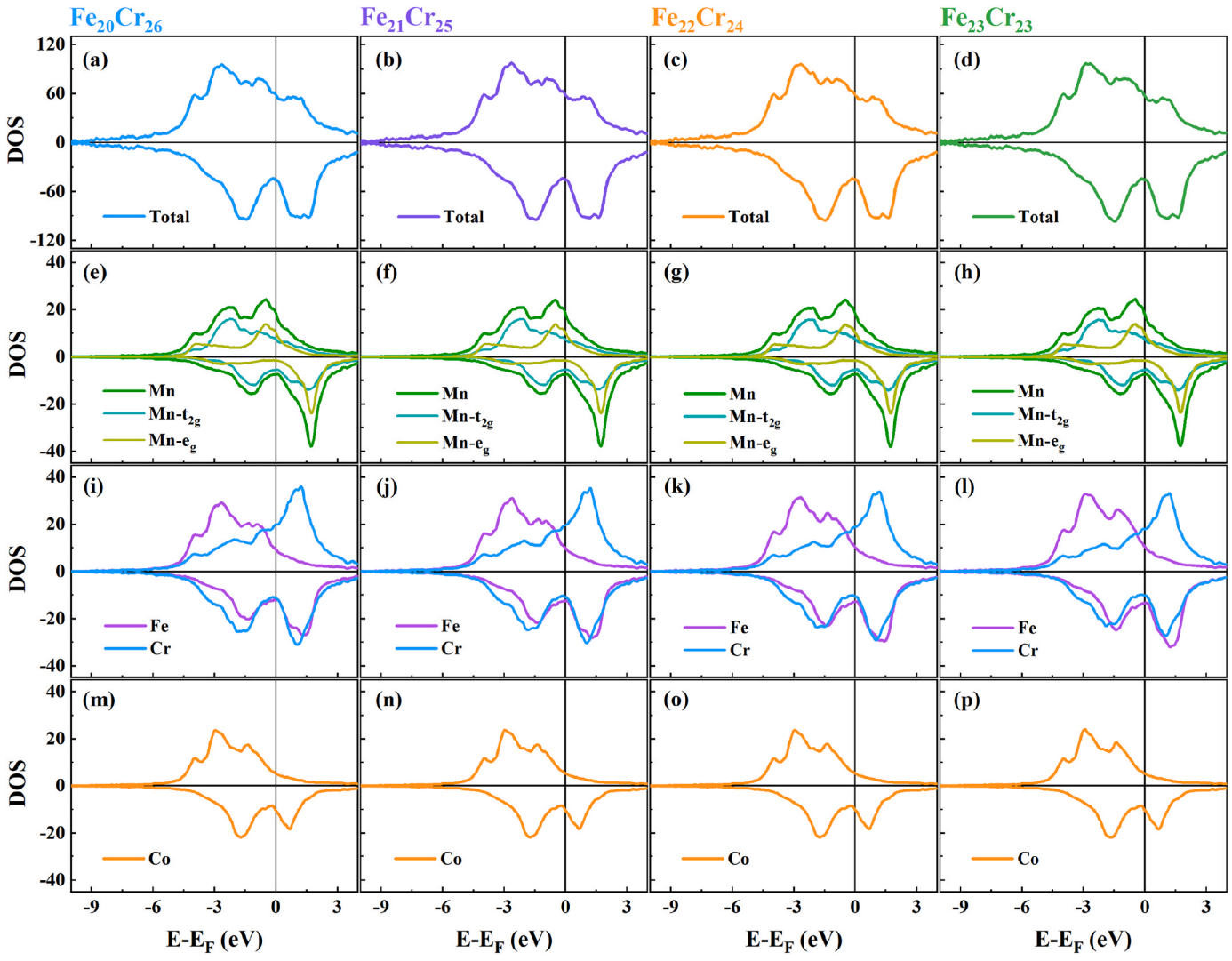

Fig. 2. The total and partial density of states (PDOS) of$Mn_{20}Al_{20}Co_{14}Fe_{20+x}Cr_{26-x}$ HE alloys.

theoretically calculated ones. The *M* increased with decreasing temperatures, implying that magnetic transition occurred in the studied compositions from a low-temperature FM to a high-temperature PM. Interestingly, a significant proportion of variation in *M* occurred and saturated at a low magnetic field ($H < 0.5$ T) in the FM state ($T < T_C$). Such a nature is favorable for practical MR practical applications. For the $Mn_{20}Al_{20}Co_{14}Fe_{20+x}Cr_{26-x}$ HE alloys, the *M*(*H*) curves coincided with each other for the heating and cooling processes. Therefore, there was no obvious hysteresis, even at low magnetic fields. The ideal reversibility in the magnetization process was desirable for MR applications. In the following, the magnetic transition characters of the $Mn_{20}Al_{20}Co_{14}Fe_{20+x}Cr_{26-x}$ HE alloys were further confirmed with the help of Arrott plots from the Banerjee criterion [49] based on the recorded *M*(*H*) curves. The corresponding Arrott plot curves for the $Fe_{20}Cr_{26}$and $Fe_{23}Cr_{23}$ HE alloys are presented in Fig. 4 (b) and (d). The positive or negative slopes in the M^2*vs. H/M* plots indicated a second/first ordered magnetic transition (SO/MT) for MC material. curves of all the measured temperatures only showed positive slopes, proving theSOMT nature of the $Mn_{20}Al_{20}Co_{14}Fe_{20+x}Cr_{26-x}$ HE alloys.

Generally, several vital and efficient figures of merit, the magnetic entropy change (ΔS_M), relative cooling power (*RCP*), and refrigerant capacity (*RC*) [50–52], could be developed from the initial assessment of the potency of the magnetocaloric material with the *M*(*H*) curves. The $\Delta S_M(T, \Delta H)$ could be reliably calculated with the Maxwell thermodynamic relation:

$$\Delta SM(T,H) = SM(T,H) - SM(T,0) = \int_0^H \left(\frac{\partial M(T,H)}{\partial T}\right) H \; dH \tag{2}$$

The ΔS_M sign for MC material strongly relied on the slope of *M* versus *T* at a given magnetic field. The *RC* was often expressed based on numerically integrating the area of $\Delta S_M(T, \Delta H)$ curves and taking the temperatures at the maximum $-\Delta S_M$ ($-\Delta S_M^{max}$) as the integration limits (T_{cold} andT_{hot}),

$$RC = \int_{Tcold}^{Thot} |\Delta SM\ (T)|\ dT \tag{3}$$

Alternatively, the *RCP* was calculated using the following equation:

$$RCP = -\Delta S_M^{max} \times \delta T^{FWHM} \tag{4}$$

where δT_{FWHM} denotes the half-maximum of $-\Delta S_M^{max}$ and equals T_{cold} -T_{hot}.

Fig. 5 presents the variation of the $-\Delta S_M$ (*T*) curves of $Mn_{20}Al_{20}$-$Co_{14}Fe_{20+x}Cr_{26-x}$ HE alloys with applied magnetic field changes (ΔH) of 0–1, 0–2, and 0–5 T. The maximum $-\Delta S_M$ ($-\Delta S_M^{max}$) values of the four studied alloys were in the vicinity of their respective Curie temperatures of approximately 268, 280, 300, and 310 K for the $Fe_{20}Cr_{26}$, $Fe_{21}Cr_{25}$, $Fe_{22}Cr_{24}$, and $Fe_{23}Cr_{23}$HE alloys, respectively. It was noted that the

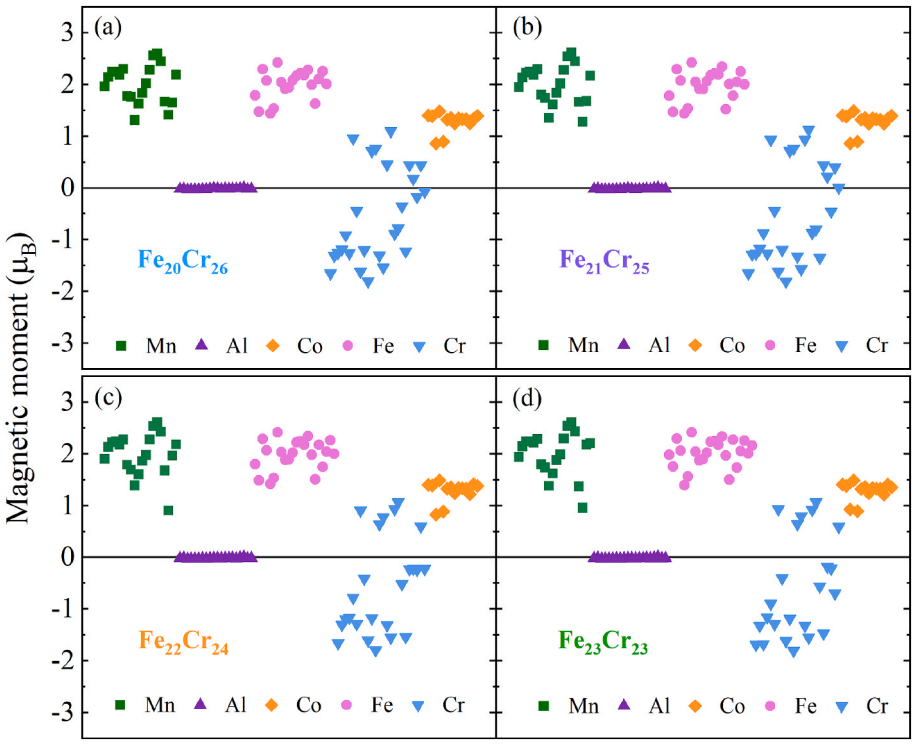

Fig. 3. The calculated magnetic moments for each element of $Fe_{20}Cr_{26}$ (a), $Fe_{21}Cr_{25}$ (b), $Fe_{22}Cr_{24}$ (c), and $Fe_{23}Cr_{23}$ (d) HE alloys, respectively.

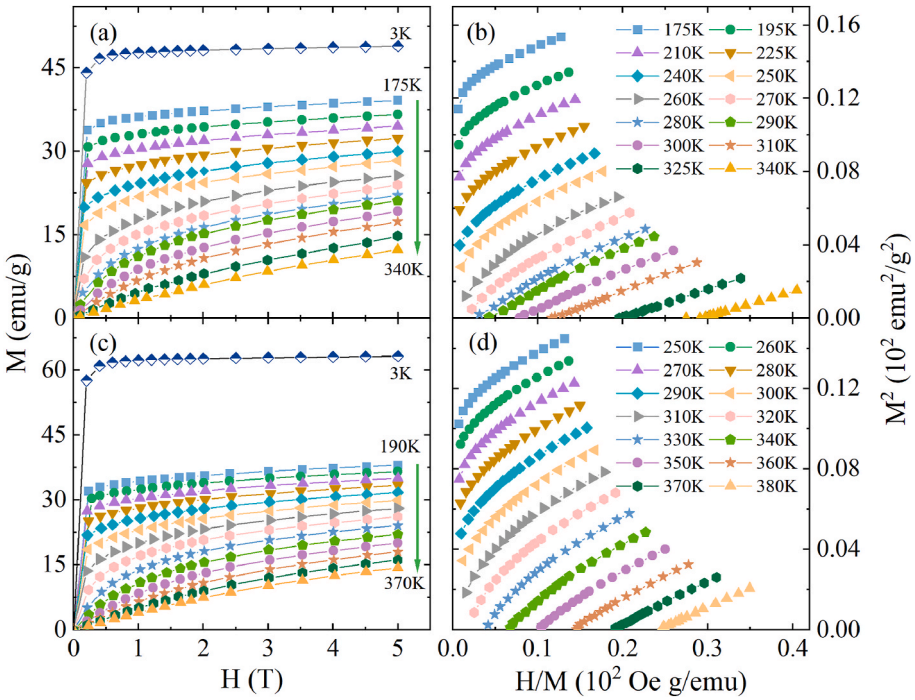

Fig. 4. The *M*(*H*) curves of $Fe_{20}Cr_{26}$ (a) and $Fe_{23}Cr_{23}$ (c)HE alloys with the corresponding Arrott plot curves of $Fe_{20}Cr_{26}$ (b) and $Fe_{23}Cr_{23}$ (d) HE alloys, respectively.

$Fe_{22}Cr_{24}$ HE alloy showed a room temperature MC effect. For ΔH of 0–2 and 0–5 T, the $-\Delta S_M^{max}$ values were calculated, based on Eq. (2), as 0.623 and 1.156 J/kgK for the $Fe_{20}Cr_{26}$ HE alloy, as 0.649 and 1.315 J/kgK for the $Fe_{21}Cr_{25}$ HE alloy, as 0.686 and 1.361 J/kgK for the $Fe_{22}Cr_{24}$ HE alloy, and as 0.662 and 1.306 J/kgK for the $Fe_{23}Cr_{23}$ HE alloy, respectively. For all the $Mn_{20}Al_{20}Co_{14}Fe_{20+x}Cr_{26-x}$ HE alloys, the $-\Delta S_M$ increased with the increasing magnetic field. Asymmetrically shaped curves were visible; in other words, the increases of high-temperature side of the peak were larger than that of low-temperature side.

Additionally, we compared the MC parameters of the $Mn_{20}Al_{20}Co_{14}Fe_{20+x}Cr_{26-x}$ HE alloys to those of well-known conventional MR materials. Despite the magnetocaloric parameters are lower than many of the reported room temperature magnetocaloric materials, such as pure Gd [3], La(Fe, Si)$_{13}$ [19], and the *RE*-based materials [4–6] as well as the FeMnNiGeSi HE alloys with magneto-structural first-order phase transition [34,35]. A detailed comparison of the magnetocaloric

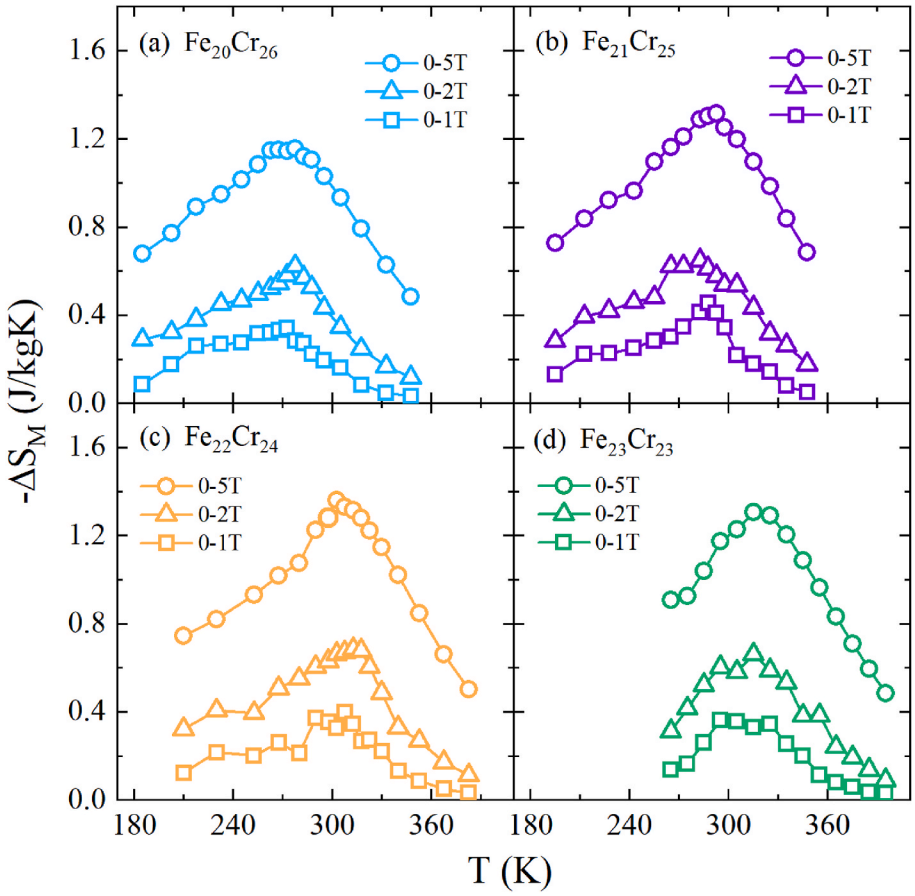

Fig. 5. The $-\Delta S_M(T)$ curvesof$Fe_{20}Cr_{26}$ (a), $Fe_{21}Cr_{25}$ (b), $Fe_{22}Cr_{24}$ (c), and $Fe_{23}Cr_{23}$ (d) HE alloys, respectively.

performances of reported HE alloys can be found in the very recently published review papers by Law et al. [30,32]. We should note that the magnetocaloric performances in the transition metal $Mn_{20}Al_{20}Co_{14}Fe_{20+x}Cr_{26-x}$ HE alloys were comparable to the reported transition metal-based magnetocaloric materials with SO-MPT around room temperature [53–59], as summarized in Fig. 6(a). Thus, let us take $Mn_{20}Al_{20}Co_{14}Fe_{22}Cr_{24}$ ($x = 2$) alloy exhibiting the $-\Delta S_M^{max}$ well-located at room temperature as one example of a detailed comparison. For the

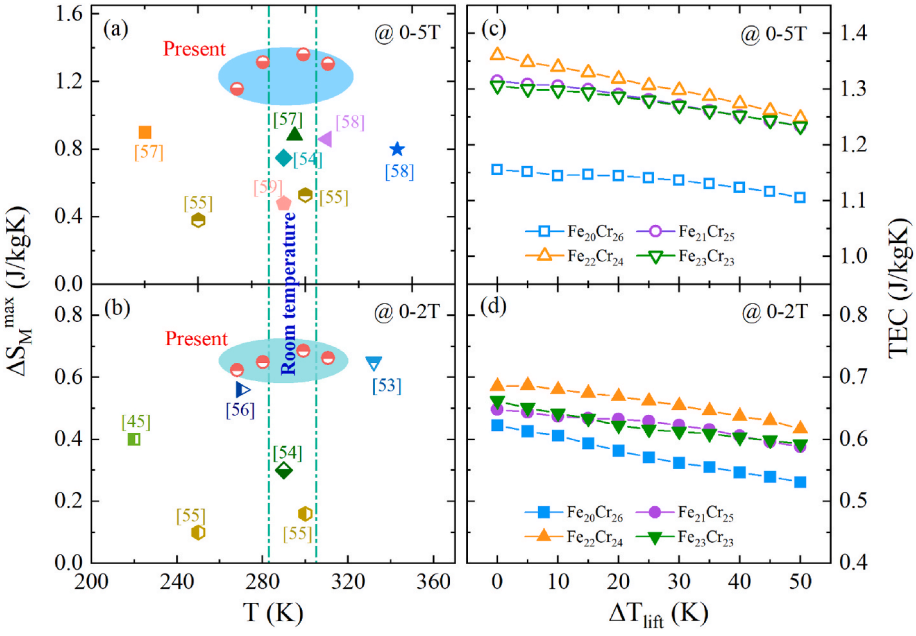

Fig. 6. (a): A comparison of $-\Delta S_M^{max}$of$Mn_{20}Al_{20}Co_{14}Fe_{20+x}Cr_{26-x}$ HE alloys and some *RE*-free MC HE alloys at an approximate around room temperature of under 0–5 T (a) and 0–2 T (b), respectively. (b): The *TEC* change of$Mn_{20}Al_{20}Co_{14}Fe_{20+x}Cr_{26-x}$ HE alloys as a function of ΔT_{lift} under 5 T (a) and 2 T (b), respectively.

magnetic field lower than 2 T, which can be realized with the commonly used NdFeB permanent magnets. Although the $-\Delta S_M^{max}$ in $Mn_{20}Al_{20}Co_{14}Fe_{22}Cr_{24}$ was lower than that of pure Gd [3,50], a larger δT_{FWHM} value of 133 K was over three times that of Gd (40 K). Therefore, the reversible $-\Delta S_M$, together with a wide working temperature zone, indicated that the $Mn_{20}Al_{20}Co_{14}Fe_{20+x}Cr_{26-x}$ HE alloys also possessed potential for practical room temperature MR applications. Moreover, the *RC* and *RCP* values were evaluated based on Eqs. (3) and (4), and the resulting values of *RC/RCP* with ΔH of 0–2 and 0–5 T were 51.80/73.22 and 150.02/189.48 J/kg for the $Fe_{20}Cr_{26}$ HE alloy, 63.79/84.56 and 152.51/197.23 J/kg for the$Fe_{21}Cr_{25}$ HE alloy, 65.56/91.17, 155.79/206.87 J/kg for the$Fe_{22}Cr_{24}$ HE alloy, and 48.30/86.74 and 127.40/159.33 J/kg for the $Fe_{23}Cr_{23}$ HE alloy, respectively. Correspondingly, the working span δT_{FWHM} was obtained with values of 117.56/163.94, 130.37/150.02, 133.01/152.02, and 131.05/122.04 K for $Fe_{20}Cr_{26}$, $Fe_{21}Cr_{25}$, $Fe_{22}Cr_{24}$, and $Fe_{23}Cr_{23}$ HE alloys under ΔH of 0–2/0–5 T, respectively.

In addition to the ΔS_M and *RC/RCP*, the temperature-averaged entropy change (*TEC*) is another index recommended for probing magnetocaloric performance [60], which is evaluated with ΔS_M (*T*) curves using the following relation:

$$TEC(\Delta Tlift) = \frac{1}{\Delta Tlift} \max_{Tmid} \left\{ \int_{Tmid-\frac{\Delta Tlift}{2}}^{Tmid+\frac{\Delta Tlift}{2}} \Delta S_M(T) \Delta H, T \; dT \right\}, \quad (5)$$

where ΔT_{lift} is the temperature range and T_{mid} is the mean central temperature that maximizes the *TEC* for a fitted value of ΔT_{lift}. In principle, $-\Delta S$ (T_{mid}) is roughly equal to *TEC* ($\Delta T_{lift} \rightarrow 0$). Therefore, the obtained *TEC* should be much more reliable regarding $-\Delta S_M^{max}$ by selecting reasonable ΔT_{lift} values. For the $Mn_{20}Al_{20}Co_{14}Fe_{20+x}Cr_{26-x}$ HE alloys, we fitted the ΔT_{lift} from 5 to 50 K with an interval of 5 K. The respective *TEC* were calculated with ΔH of 0–2 and 0–5 T, as presented in Fig. 6(b). The *TEC* values gradually and slowly decreased with increasing ΔT_{lift} for the $Mn_{20}Al_{20}Co_{14}Fe_{20+x}Cr_{26-x}$ HE alloys. The resulting *TEC* values with a ΔT_{lift} of 50 K under ΔH of 0–2/0–5 Twere 0.531/1.106 for the $Fe_{20}Cr_{26}$HE alloy, 0.588/1.234 for the $Fe_{21}Cr_{25}$HE alloy, 0.617/1.248 for the $Fe_{22}Cr_{24}$ HE alloy, and 0.592/1.233 for the $Fe_{23}Cr_{23}$HE alloy, respectively. These values versus their respective $-\Delta S_M^{max}$ [that is *TEC* ($\Delta T_{lift} \rightarrow 0$)] at the same ΔH of 0–2/0–5 T can reach 85.3/95.7%, 90.7/93.9%, 90.0/91.7%, and 89.5/94.4% for the $Fe_{20}Cr_{26}$, $Fe_{21}Cr_{25}$, $Fe_{22}Cr_{24}$, and $Fe_{23}Cr_{23}$HE alloys. These higher percentages demonstrated that $Mn_{20}Al_{20}Co_{14}Fe_{20+x}Cr_{26-x}$ HE alloys could be properly operated as magnetic refrigerants with a wide working span of approximately 50 K, which is more representative of magnetocaloric performance evaluation.

Moreover, the mechanical properties of the $Mn_{20}Al_{20}Co_{14}Fe_{20+x}Cr_{26-x}$ HE alloys was also determined at room temperature, and the resulting compressive stress-strain curves are shown in Fig. 7. We can note that the stress and strain in the $Fe_{20}Cr_{26}$ HE alloy were lower than in the $Fe_{21}Cr_{25}$, $Fe_{22}Cr_{24}$ and $Fe_{23}Cr_{23}$HE alloys. This finding indicates that the addition of Fe helped increase strength of the alloys. The obtained maximum compressive strength of approximately 240 Mpa was much higher than that of most typical giant magnetocaloric materials, such as epoxy-bonded $Mn_{0.98}CoGe$ (152 MPa) [61] and hot-pressed $LaFe_{11.6}Si_{1.4}H_y$/Sn (170 MPa) [62]. Meanwhile, it was comparable with those of epoxy-bonded $La_{1.7}Fe_{11.6}Si_{1.4}$ (272 MPa) [63] and within the range of pure Gd (160–300 MPa) [3]. The improved mechanical properties, along with the amazing working around room temperature, make the $Mn_{20}Al_{20}Co_{14}Fe_{20+x}Cr_{26-x}$ HE alloys suitable for practical room temperature MR applications.

4. Conclusions

In summary, the transition metal HE alloys $Mn_{20}Al_{20}Co_{14}Fe_{20+x}Cr_{26-x}$($x$ = 0, 1, 2, 3) were fabricated and systematically investigated with regards to their structural, magnetic, magnetocaloric and mechanical properties by means of experimental determination and first principle calculations. The $Mn_{20}Al_{20}Co_{14}Fe_{20+x}Cr_{26-x}$ HE alloys were crystallized in a disordered bcc structure. The substitution of Fe by Cr continuously raised the magnetic transition temperature to around room temperature, *i. e.*, 299.2 K for $Fe_{22}Cr_{24}$ and 280.3 K for $Fe_{21}Cr_{25}$ HE alloys. The partial DOS and magnetic moment of individual specific elements were evaluated with DFT calculation. The Mn, Co, and Fe elements exhibited ferromagnetic behavior, whereas Cr substantially reduced net magnetic moments.The magnetocaloric performances of $Mn_{20}Al_{20}Co_{14}Fe_{20+x}Cr_{26-x}$ HE alloys were examined using the parameters of magnetic entropy changes, relative cooling powders, refrigerant capacity, and temperature average entropy change, which are comparable with the reported transition metal-based magnetocaloric materials with SO-MPT. By considering the benefits of transition metal HE alloys, such as, low price of raw materials, easy to be fabricated, high physical/chemical stabilities, promising mechanical properties, the present $Mn_{20}Al_{20}Co_{14}Fe_{20+x}Cr_{26-x}$ HE alloys are also considerable for practical room temperature MR applications. The present work would provide a large family of transition metal HE alloys with considerable magnetocaloric performances.

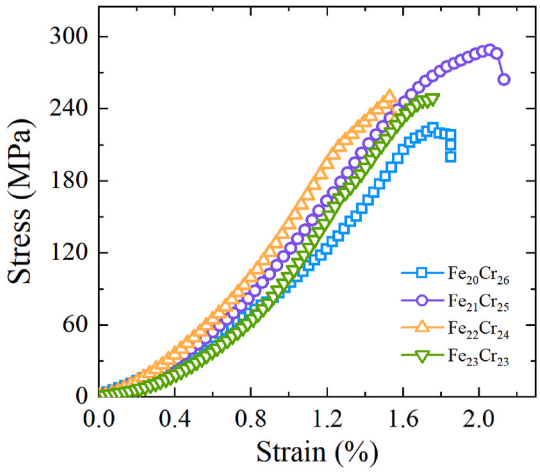

Fig. 7. The compressive stress-strain curves of the $Mn_{20}Al_{20}Co_{14}Fe_{20+x}Cr_{26-x}$ HE alloys.

Authorship contribution statement

Yikun Zhang: Methodology, Validation, Investigation, Supervision, Project administration, Writing - original draft. **Peng Xu**: Investigation, Methodology, Formal analysis, Data curation. **Jian Zhu**: Investigation, Validation, Data curation. **Shiming Yan**: Methodology, Writing - review & editing. **Jincang Zhang**: Conceptualization, Writing - review & editing. **Lingwei Li**: Conceptualization, Formal analysis, Software, Methodology, Project administration, Writing - review & editing.

Declaration of competing interest

The authors declare that they have no known competing financial interests or personal relationships that could have appeared to influence the work reported in this paper.

Data availability

Data will be made available on request.

Acknowledgments

The present work was supported by the National Natural Science

Foundation of China (Grant No. 52071197) and Key Research Project of Zhejiang Laboratory (Grant No. 2021PE0AC02). The authors acknowledge the Supercomputing Center of Hangzhou Dianzi University for providing computing resources.

References

[1] X. Moya, S. Kar-Narayan, N.D. Mathur, Caloric materials near ferroic phase transitions, Nat. Mater. 13 (2014) 439–450.

[2] I. Takeuchi, K. Sandemana, Solid-state cooling with caloric materials, Phys. Today 68 (2015) 48–54.

[3] V. Franco, J.S. Blázquez, J.J. Ipus, J.Y. Law, L.M. Moreno-Ramírez, A. Conde, Magnetocaloric effect: from materials research to refrigeration devices, Prog. Mater. Sci. 93 (2018) 112–232.

[4] Y.K. Zhang, Y. Tian, Y. Jia, Z. Zhang, S. Li, B. Zhang, J. Wang, Z. Ren, Magnetic properties and giant cryogenic magnetocaloric effect in *B*-site ordered antiferromagnetic Gd_2MgTiO_6 double perovskite oxide, Acta Mater. 226 (2022): 117669.

[5] L.W. Li, M. Yan, Recent progress in the development of $RE_2TMTM'O_6$ double perovskite oxides for cryogenic magnetic refrigeration, J. Mater. Sci. Technol. 136 (2023) 1–12.

[6] P. Xu, Z.P. Ma, P. Wang, H. Wang, L.W. Li, Excellent cryogenic magnetocaloric performances in ferromagnetic Sr_2GdNbO_6 double perovskite compound, Mater. Today Phys. 20 (2021): 100470.

[7] Y. Wang, L. Wang, J. Xia, Z. Lai, G. Tian, X. Zhang, Z. Hou, X. Gao, W. Mi, M. Zeng, G. Zhou, G. Yu, G. Wu, Y. Zhou, W. Wang, X.X. Zhang, J.M. Liu, Electric-field-driven non-volatile multi-state switching of individual skyrmions in a multiferroic heterostructure, Nat. Commun. 11 (2020) 3577.

[9] Y.D. Wang, Z.J. Wei, H.R. Tu, C.H. Zhang, Z.P. Hou, Electric field manipulation of magnetic skyrmions, Rare Metals 41 (2022) 4000–4014.

[10] H. Wang, T.N. Lamichhane, M.P. Paranthaman, Review of additive manufacturing of permanent magnets for electrical machines: a prospective on wind turbine, Mater. Today Phys. 24 (2022): 100675.

[11] Y. Zhang, J. Zhu, S. Li, Z. Zhang, J. Wang, Z. Ren, Magnetic properties and promising cryogenic magnetocaloric performances in the antiferromagnetic $GdFe_2Si_2$ compound, Sci. China Mater. 65 (2022) 1345–1352.

[12] Z. Ma, X. Dong, Z. Zhang, L. Li, Achievement of promising cryogenic magnetocaloric performances in $La_{1-x}Pr_xFe_{12}B_6$ compounds, J. Mater. Sci. Technol. 92 (2021) 138–142.

[13] J.Y. Law, V. Franco, L.M. Moreno-Ramírez, A. Conde, D.Y. Karpenkov, I. Radulov, K.P. Skokov, O. Gutfleisch, A quantitative criterion for determining the order of magnetic phase transitions using the magnetocaloric effect, Nat. Commun. 9 (2018) 2680.

[14] B. Shen, J. Sun, F. Hu, H. Zhang, Z. Cheng, Recent progress in exploring magnetocaloric materials, Adv. Mater. 21 (2009) 4545–4564.

[15] Y. Zhang, S. Li, L. Hu, X. Wang, L. Li, M. Yan, Excellent magnetocaloric performance in the carbide compounds $RE_2Cr_2C_3$ (*RE* = Er, Ho, and Dy) and their composites, Mater. Today Phys. 27 (2022): 100786.

[16] P. Xu, L. Hu, Z. Zhang, H. Wang, L. Li, Electronic structure, magnetic properties and magnetocaloric performance in rare earths (RE) based RE_2BaZnO_5 (*RE* = Gd, Dy, Ho, and Er) compounds, Acta Mater. 236 (2022): 118114.

[17] Z. Hou, L. Li, C. Liu, X. Gao, Z. Ma, Y. Peng, M. Yan, X. Zhang, J. Liu, Emergence of room temperature stable skyrmionic bubbles in the rare earth based $REMn_2Ge_2$ (*RE* = Ce, Pr, and Nd) magnets, Mater. Today Phys. 17 (2021): 100341.

[18] Y. Li, L. Qin, S. Huang, L.W. Li, Enhanced magnetocaloric performances and tunable martensitic transformation in $Ni_{35}Co_{15}Mn_{35-x}Fe_xTi_{15}$ all-d-metal Heusler alloys by chemical and physical pressures, Sci. China Mater. 65 (2022) 486–493.

[19] Y. Liu, X. Fu, Q. Yu, M. Zhang, J. Liu, Significant reduction of phase-transition hysteresis for magnetocaloric $(La_{1-x}Ce_x)_2Fe_{11}Si_2H_y$ alloys by microstructural manipulation, Acta Mater. 207 (2021): 116687.

[20] J.Q. Feng, Y.H. Liu, J.H. Sui, A.N. He, W.X. Xia, W.H. Wang, J.Q. Wang, J.T. Huo, Giant refrigerant capacity in Gd-based amorphous/nanocrsytalline composite fibers, Mater. Today Phys. 21 (2021): 100528.

[21] D. Guo, L.M.M. Ramírez, J.Y. Law, Y.K. Zhang, V. Franco, Excellent cryogenic magnetocaloric properties in heavy rare-earth based $HRENiGa_2$ (HRE = Dy, Ho or Er) compounds, Sci. China Mater. 66 (2023) 249–256.

[22] X.X. Wang, W.Q. Wang, W.D. Hutchison, F. Su, Y.F. Xue, C.W. Wang, W. Sun, J. M. Cadogan, S.J. Campbell, Z.X. Cheng, J.L. Wang, Plateau-like magnetocaloric effect in layered intermetallic compounds activated by tripled magnetic cell, Mater. Today Phys. 21 (2021): 100501.

[23] J. Yeah, S. Cheng, S. Lin, J. Gan, T. Ching, T. Shun, C.H. Tseau, S. Chan, Nanostructured high-entropy alloys with multiple principal elements: novel alloy design concepts and outcomes, Adv. Eng. Mater. 6 (2004) 299–303.

[24] Y. Zhang, T. Tang, M. Gan, K. Dahmeen, P. Liaw, Z. Luo, Microstructures and properties of high-entropy alloys, Prog. Mater. Sci. 61 (2014) 1–93.

[25] D.B. Miracle, O.N. Senkov, A critical review of high entropy alloys and related concepts, Acta Mater. 122 (2017) 448–511.

[26] E.P. George, D. Raabe, R.O. Ritchie, High-entropy alloys, Nat. Rev. Mater. 4 (2019) 515–534.

[27] E.P. George, W.A. Curtin, C.C. Tasan, High entropy alloys: a focused review of mechanical properties and deformation mechanisms, Acta Mater. 188 (2020) 435–474.

[28] Y. Yuan, Y. Wua, X. Tong, H. Wan, Z. Liu, H. Suog, Z. Liu, Rare-earth high-entropy alloys with giant magnetocaloric effect, Acta Mater. 125 (2017) 481–489.

[29] Y. Zhang, J. Zhu, S. Li, J. Wang, Z. Ren, Achievement of giant cryogenic refrigerant capacity in quinary rare-earths based high-entropy amorphous alloy, J. Mater. Sci. Technol. 102 (2022) 66–71.

[30] J.Y. Law, V. Franco, Review on magnetocaloric high-entropy alloys: design and analysis methods, J. Mater. Res. 38 (2022) 37–51.

[31] H. Yin, J.Y. Law, Y.J. Huang, H.X. Shen, S. Jiang, S. Guo, V. Franco, J. Sun, Enhancing the magnetocaloric response of high-entropy metallic-glass by microstructural control, Sci. China Mater. 65 (2022) 1134–1142.

[32] J.Y. Law, V. Franco, Pushing the limits of magnetocaloric high-entropy alloys, Apl. Mater. 9 (2021): 080702.

[33] H. Yin, J.Y. Law, Y.J. Huang, V. Franco, H.X. Shen, S. Jiang, Y. Bao, J. Sun, Design of Fe-containing GdTbCoAl high-entropy-metallic-glass composite microwires with tunable Curie temperatures and enhanced cooling efficiency, Mater. Des. 206 (2021): 109824.

[34] J.Y. Law, Á. Díaz-García, L.M. Moreno-Ramírez, V. Franco, Increased magnetocaloric response of FeMnNiGeSi high-entropy alloys, Acta Mater. 212 (2021): 116931.

[35] J.Y. Law, L.M. Moreno-Ramírez, Á. Díaz-García, A. Matin-Cid, S. Kobayashi, T. Nakamura, V. Franco, MnFeNiGeSi high-entropy alloy with large magnetocaloric effect, J. Alloys Compd. 855 (2021): 157424.

[36] A. Tekgül, K. Sarlar, N. Küçük, A.B. Etemoğlu, The structural, magnetic and magnetocaloric properties of MnCrNiGeSi high-entropy alloy, Phys. Scripta 97 (2022): 075814.

[37] K. Sarlar, A. Tekgül, N. Küçük, A.B. Etemoğlu, Structural and magnetocaloric properties of FeNi high entropy alloys, Phys. Scripta 96 (2021): 125847.

[38] M.C. Haciismailoglu, K. Sarlar, A. Tekgül, I. Kucuk, Thermally evaporated FeMGaMnSi (M = Co, Ni) high entropy alloy thin films: magnetic and magnetoresistance properties, J. Non-Cryst. Solids 539 (2020): 120063.

[39] K. Sarlar, Atakan Tekgül, I. Kucuk, Magnetocaloric properties of rare-earth-free $Mn_{27}Cr_7Ni_{33}Ge_{25}Si_8$ high-entropy alloy, IEEE Magn. Lett. 10 (2019): 2109905.

[40] G. Kresse, J. Furthmüller, Efficient iterative schemes for ab initiototal-energy calculations using a plane-wave basis set, Phys. Rev. B 54 (1996) 11169–11186.

[41] J.P. Perdew, K. Burke, M. Ernzerhof, Generalized gradient approximation madesimple, Phys. Rev. Lett. 77 (1996) 3865–3868.

[42] G. Kresse, D. Joubert, From ultrasoft pseudopotentials to the projector augmented-wave method, Phys. Rev. B 59 (1999) 1758–1775.

[43] R. Wei, H. Zhang, H. Wang, C. Chen, T. Wang, F. Li, S. Guan, T. Zhang, T. Hu, Y. Dong, J. Alloys Compd. 789 (2019) 762–767.

[44] C. Jung, K. Kang, A. Marshal, K.G. Pradeep, J.B. Seol, H.M. Lee, P.P. Choi, Effects of phase composition and elemental partitioning on soft magnetic properties of AlFeCoCrMn high entropy alloys, Acta Mater. 171 (2019) 31–39.

[45] J. Harris, Z. Leong, P. Gong, J. Cornide, C. Pughe, T. Hansen, A. Quintana-Nedelcos, R. Rowan-Robinson, U. Dahlborg, M. Calvo-Dahlborg, R. Goodall, M. Rainforth, N. Morley, Investigation into the magneticproperties of CoFeNiCryCux alloys, J. Phys. D Appl. Phys. 54 (2021): 395003.

[46] C. Wagner, A. Ferrari, J. Schreuer, J.-P. Couzinié, Y. Ikeda, F. Körmann, G. Eggeler, E.P. George, G. Laplanche, Effects of Cr/Ni ratio on physical properties of Cr-Mn-Fe-Co-Ni high-entropy alloys, Acta Mater. 227 (2022): 117693.

[47] X.Z. Liang, J. Bai, J.L. Gu, J.L. Wang, H.L. Yan, Y.D. Zhang, C. Esling, X. Zhao, L. Zuo, Ab initio-based investigation of phase transition path and magnetism of Ni–Mn–In alloys with excess Ni or Mn, Acta Mater. 195 (2020) 109–122.

[48] Z.Q. Guan, J. Bai, Y. Zhang, J.L. Gu, X.J. Jiang, X.Z. Liang, R.K. Huang, Y.D. Zhang, C. Esling, X. Zhao, L. Zuo, Revealing essence of magnetostructural coupling of Ni-Co-Mn-Ti alloys by first-principles calculations and experimental verification, Rare Met. 41 (2022) 1933–1947.

[49] B.K. Banerjee, On a generalised approach to first and second order magnetic transitions, Phys. Lett. 12 (1964) 16–17.

[50] K.A. Gschneidner, V.K. Pecharsky, A.O. Tsokol, Recent developments in magnetocaloric materials, Rep. Prog. Phys. 68 (2005) 1479–1539.

[51] L. Li, M. Yan, Recent progresses in exploring the rare earth based intermetallic compounds for cryogenic magnetic refrigeration, J. Alloys Compd. 823 (2020): 153810.

[52] Z.P. Ma, P. Xu, J.Y. Ying, Y.K. Zhang, L.W. Li, Insight into the structural and magnetic properties of $RECo_{12}B_6$ (*RE* = Ce, Pr, Nd)compounds: a combined experimental and theoretical investigation, Acta Mater. 247 (2023): 118757.

[53] K. Sarlara, A. Tekgüla, I. Kucuk, Magnetocaloric properties in a FeNiGaMnSi high entropy alloy, Curr. Appl. Phys. 20 (2020) 18–22.

[54] B.G.F. Eggert, E.K. Delczeg-Czirjak, F. Maccari, S. Kumar, O. Gutfleisch, H. Fjellvåg, B.C. Hauback, C. Frommen, Exploring V-Fe-Co-Ni-Al and V-Fe-Co-Ni-Cu high entropy alloys formagnetocaloric applications, J. Alloys Compd. 921 (2022): 166040.

[55] S. Vorobiov, O. Pylypenko, Yu Bereznyak, I. Pazukha, E. Čižmár, M. Orendáč, V. Komanicky, Magnetic properties, magnetoresistive, and magnetocaloriceffects of AlCrFeCoNiCu thin-film high-entropy alloys preparedby the co-evaporation technique, Appl. Phys. A 127 (2021) 179.

[56] A. Quintana-Nedelcos, Z. Leong, N.A. Morley, Study of dual-phase functionalisation of NiCoFeCr-Al_xmulticomponent alloys for the enhancement of magnetic propertiesand magneto-caloric effect, Mater. Today Energy 20 (2021): 100621.

[57] D. Belyea, M. Lucas, E. Michel, J. Horwath, C.W. Miller, Tunable magnetocaloric effect intransition metal alloys, Sci. Rep. 5 (2015): 15755.

[58] Y. Zhang, K. Han, M. Li, M. Gao, X. Wang, G. Wang, J.Q. Wang, J. Huo, Design of Co-based amorphous alloys with magnetocaloric effect nearroom temperature, J. Non-Crys. Solids 592 (2022): 121763.

[59] S.-M. Na, P.K. Lambert, H. Kim, J. Paglione, N.J. Jones, Thermomagnetic properties and magnetocaloric effect of FeCoNiCrAl-type high-entropy alloys, AIP Adv. 9 (2019): 035010.
[60] L.D. Griffith, Y. Mudryk, J. Slaughter, V.K. Pecharsky, Material-based figure of merit for caloric materials, J. Appl. Phys. 123 (2018): 034902.
[61] F. Zhu, J. Lin, W. Jiang, C. Yang, L. Li, X. Zhang, W. Song, X. Zhu, P. Tong, Y. Sun, Enhanced mechanical properties and large magnetocaloric effect inepoxy-bonded $Mn_{0.98}CoGe$, Scripta Mater. 150 (2018) 96.
[62] H. Zhang, J. Liu, M. Zhang, Y. Shao, Y. Li, A. Yan, $LaFe_{11.6}Si_{1.4}Hy$/Sn magnetocaloric composites by hot pressing, Scripta Mater. 120 (2016) 58–61.
[63] S. Kavita, M. Alagusoundarya, V.V. Ramakrishna, V. Suresh, Pramod Bhatt, P. Srimathi, R. Archana, D. Kar, T. Thomas, R. Gopalan, On the table-like magnetocaloric effect, microstructure and mechanicalproperties of $La_xFe_{11.6}Si_{1.4}$ system, J. Alloys Compd. 895 (2022): 162597.